THE JOURNAL OF PHYSICAL CHEMISTRY LETTERS
A JOURNAL OF THE AMERICAN CHEMICAL SOCIETY

Editors' Choice
Open Access

pubs.acs.org/JPCL

Letter

Nanosecond-Lived Excimer Observation in a Crystal of a Rhodium(I) Complex via Time-Resolved X-ray Laue Diffraction

Piotr Łaski, Lerato Bosman, Jakub Drapała, Radosław Kamiński, Dariusz Szarejko, Patryk Borowski, Andreas Roodt, Robert Henning, Alice Brink,* and Katarzyna N. Jarzembska*

Cite This: J. Phys. Chem. Lett. 2024, 15, 10301−10306

Read Online

ABSTRACT: The rare observation of transient Rh···Rh excimer formation in a single crystal is reported. The estimated excited-state lifetime at 100 K is 2 ns, which makes it the shortest-lived small-molecule species caught experimentally using the laser-pump/X-ray-probe time-resolved Laue method. Upon excitation with 390 nm laser light, the intermolecular Rh···Rh distance decreases from 3.379(4) to 3.19(1) Å, and the metal−metal contact gains more bonding character. On the basis of the experimental results and theoretical modeling, the structural changes determined with 100 ps time resolution reflect principally the $S_0 \rightarrow S_1$ electronic transition.

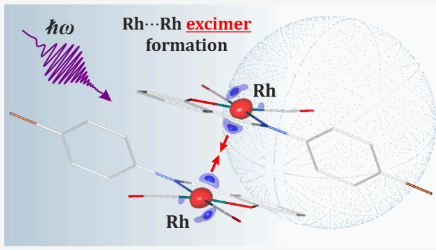

Profound investigations of light−matter interactions are indispensable for understanding the mechanisms of crucial (bio)chemical processes, the nature of excited states, and structural dynamics. Such knowledge can be successfully applied to the design of novel effective functional materials for applications in optoelectronics, solar energy conversion systems, storage devices, sensors, etc.[1−5] Because many such materials are solid-state materials, conducting studies using their applicable form or at least as a simplified model would be desirable. In this respect, crystals constitute convenient model systems, as they can be relatively easily studied using crystallographic methods. Nevertheless, to trace short-lived transient species, advanced approaches have to be applied, such as laser-pump/X-ray-probe methods combined with serial crystallography,[6−8] or the "pink"-beam Laue technique.[9−14] To achieve the required fine time resolution, such experiments are performed at synchrotron or XFEL sources, where ultrashort (approximately femtoseconds to picoseconds) X-ray pulses can be generated. A number of studies of this kind have already been conducted for macromolecular samples;[13,15−20] however, due to the development of data analysis tools, some small-molecule crystals have also been quite successfully examined to date.[9,10,12,21−34]

In this work, we have focused our attention on a newly synthesized rhodium(I)-based potential precatalyst (hereafter **Rh-4-Br**) for model Monsanto reactions.[35−38] The rhodium Monsanto process has played a significant role in the homogeneous catalytic reaction involving the carbonylation of methanol to acetic acid with an annual global use of several million tons of acetic acid.[39−41]

The distorted-square-planar molecular structure of **Rh-4-Br** is shown in Figure 1a. The rhodium atom is coordinated by two carbonyl groups and by a monoanionic N,O-donor bidentate ligand. The phenyl ring connected to the N1 atom

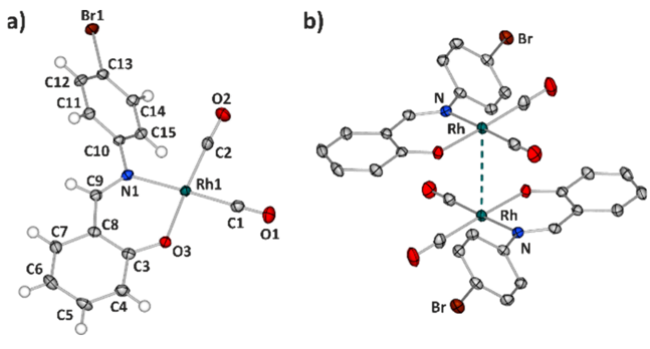

Figure 1. (a) Molecular structure of **Rh-4-Br**. (b) Main dimeric motif in the crystal structure of **Rh-4-Br** [note the Rh···Rh distance is 3.379(4) Å]. Thermal motion is shown as ellipsoids at the 50% probability level.

is substituted with a bromine atom in the *para* position. The compound crystallizes in space group $P2_1/n$, with one molecule in the asymmetric unit. The strongest interacting dimeric motif in the solid state is illustrated in the crystal structure, characterized by an interaction energy of approximately −74 kJ mol^{-1} (Table S3.2), as shown in Figure 1b. It consists of two center-of-symmetry-related molecules and is stabilized mainly by the d^8−d^8 (d_{z^2}-type) Rh···Rh metallophilic contact [metal−metal distances of 3.379(4) Å] and two C15−H15···O3 hydrogen-bond-type interactions between the

Received: August 23, 2024
Revised: September 24, 2024
Accepted: September 27, 2024

https://doi.org/10.1021/acs.jpclett.4c02476
J. Phys. Chem. Lett. 2024, 15, 10301−10306

bromine-substituted phenyl rings and the oxygen atom from the Rh coordination sphere of the adjacent molecule. Importantly, these dimers constitute discrete motifs in the crystal structure (Figure S2.1a), as the Rh···Rh interactions do not propagate further in space, a rare occurrence for many complexes of this type.[42,43] The other side of the metal center is surrounded by two bromine atoms of the two molecules located above (Supporting Information).

The shortest intermolecular Rh···Br distances amount to 4.206(5) and 4.348(5) Å, and the interaction energies of the respective dimers, stabilized also by hydrogen-bond-type interactions, are equal to −26.3 and −40.9 kJ mol^{-1}, respectively. With respect to the crystal architecture, slightly undulated molecular layers parallel to the $(\bar{1}03)$ crystal plane can be distinguished (Figure S2.1b).

Platinum-group transition-metal coordination compounds often exhibit interesting spectroscopic behavior, which can be significantly affected by the metallophilic interactions if formed.[44−48] The luminescence shown by **Rh-4-Br** can also, to some extent, be associated with the d_{z^2}-type Rh···Rh contacts. Fluorescence is rather weak in the solid state, with the maximum at ~560 nm (Table 1). The estimated lifetime of the emissive state is <1 ns at room temperature (~700 ps) and increases with a decrease in temperature reaching ~2 ns at 100 K. No thermally activated delayed fluorescence (TADF)[49] was detected (Supporting Information).

Table 1. Solid-State Emission Maxima and Lifetimes for Rh-4-Br

temperature, T (K)	emission maximum, λ_{em}^{max} (nm)	emission lifetime, τ (ns)
room temperature	566	0.70(1)
250	561	0.77(1)
200	558	1.25(1)
150	558	1.70(1)
100	557	2.01(1)

The theoretical computations were performed by using the density functional theory (DFT) method (Supporting Information). The used range-separated CAM-B3LYP functional[50] should take into account possible charge transfer occurring upon excitation, which is important once a dimeric motif is considered. According to the time-dependent DFT-derived vertical electronic transitions, the lowest singlet−singlet transition occurs at ~360 nm. It involves a number of molecular orbitals with the most significant contributions from the HOMO−2 → LUMO and HOMO−2 → LUMO+2 transitions, and noteworthy HOMO → LUMO and HOMO → LUMO+2 components (Figure S3.1). The HOMO−2 orbital is located principally on the Rh centers (mainly d_{z^2} atomic orbitals) and has an antibonding character. HOMO also covers the Rh atomic orbitals and has a similar antibonding nature; however, it is additionally visibly spread over the heterocyclic ligand fragment. In turn, the LUMO orbital involves the heterocyclic fragment of the ligand, and to a lesser extent the Rh atomic orbitals (mainly d_{xy}), whereas LUMO+2 shows more emphasized metal−metal bond character (Figure S3.1f). Overall, the $S_0 \rightarrow S_1$ electronic transition is a mixture of $\pi \rightarrow \pi^*$ excitation and metal-to-ligand charge transfer (MLCT) with a metal-to-metal bond CT contribution. Relatively close in energy, at ~345 nm, a similar in nature but brighter $S_0 \rightarrow S_3$ transition can be found (Table S3.1). In this case, the MLCT character is much more dominant. Also, the lowest-energy singlet−triplet transition ($S_0 \rightarrow T_1$, ~476 nm) resembles the $S_0 \rightarrow S_3$ transition in character, though it lacks contributions from HOMO−2 and LUMO+2 involving the Rh···Rh region most. The calculated ultraviolet−visible spectrum well reflects features of the respective experimental solid-state data (Figure S4.1). The latter is more spread out and shifted toward lower energies, which is typical for solid-state absorption spectra.

In light of the information presented above, we expect some structural changes in the central region of the studied molecule once the system is excited with the 390 nm laser light matching the experimental solid-state band with respect to the $S_0 \rightarrow S_1$ electronic transition. Thus, the time-resolved (TR) laser-pump/X-ray-probe Laue diffraction experiment was carried out at the BioCARS beamline in APS, allowing for ~100 ps single-X-ray-pulse diffraction.[20,51] The X-ray diffraction signals were collected both after ("ON", pump−probe delay set to 100 ps; laser-pulse duration of 38 ps) and without ("OFF") laser exposure, while further data treatment was based on the intensity ratios ($R_{ON/OFF} = I_{ON}/I_{OFF}$).[52] The collected data were integrated using our GPU-accelerated one-dimensional seed-skewness algorithm (Supporting Information).[53] Further processing[24,54−59] and merging of four best-quality data sets yielded a single data set of ~50% overall completeness. Due to the relatively small excimer population, charge density changes can be reliably assessed only fairly close to the heavy atoms (here Rh and Br atoms), while the statistical noise and Fourier-rippling effects for less complete data sets overshadow the possible signal in the remaining part of the molecule (for details, see the Supporting Information). The resulting photodifference map[60,61] ($F_{ON}^{100\ ps} - F_{OFF}$) illustrating the observed electron density changes upon laser light excitation is presented in Figure 2.

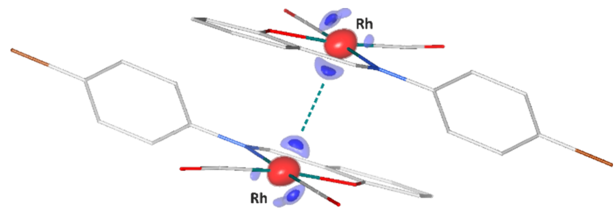

Figure 2. Photodifference map ($F_{ON}^{100\ ps} - F_{OFF}$) of **Rh-4-Br** showing atomic shifts in the S_1 excited state superimposed onto the S_0 ground-state geometry. Solid isosurfaces, ±0.50 e Å^{-3}; semitransparent, ±0.41 e Å^{-3}; blue for positive and red for negative.

The significant accumulation of electrons in the region between the two Rh centers and typical depletion of electron density at atomic positions suggest temporary contraction of the metal−metal bond after excitation and increased vibration of all atoms due to the laser-induced increase in temperature. A weaker signal on the other side of the metal center in the direction of the neighboring Br atom can be related to a shift of both the adjacent molecules toward each other upon excitation (Figure S5.3). Indeed, it is also accompanied by accumulation of some electron density at the respective side of the Br atom. Pairs of closest bromine atoms also seem to move slightly toward each other upon excitation. It should also be noted that on the basis of the photo-Wilson plot analysis,[62−64] the increase in temperature upon excitation was estimated to be ~4 K (Figure S5.6).

https://doi.org/10.1021/acs.jpclett.4c02476
J. Phys. Chem. Lett. 2024, 15, 10301−10306

To determine the experimental geometry of the short-lived excited-state species and verify the presumptions described above, a response ratio [$\eta = (I_{ON} - I_{OFF})/I_{OFF} = R_{ON/OFF} - 1$] structure refinement was conducted.[65−67] Given the moderate data completeness, it was crucial to first estimate the population of the excited state so it can be set at a fixed value during further refinement steps. An excited-state population of 1% assures the lowest discrepancy ratio-based R_R factor[68] (Figure S5.4), whereas the most reasonable results were obtained when only the Rh atoms were refined freely. Such an approach is sensible, taking into account the very small excited-state population and data completeness. As a result, a notable signal is obtained only for electron-rich heavy atoms such as Rh or Br. Indeed, apart from the electron density peaks in the vicinity of the Rh centers, some significant electron density redistribution is also visible for the bromine atoms. However, the refinement of Br strongly affects the position of the organic part of the molecule that cannot be refined reliably (Supporting Information). In all of the tested structural models, the Rh···Rh contact shortens significantly. The intermolecular Rh···Rh distance decreases from 3.379(4) to 3.19(1) Å (i.e., by ∼6%) in the most trustworthy model, leading to metallophilic interaction strengthening and formation of the excimer species. The character of this transition, spectroscopic features, and structural changes are in agreement with the time-dependent DFT results for the $S_0 \rightarrow S_1$ transition and the QM/MM modeling (Figure S3.3).[69] Its nature is illustrated well by the transition density map and atomic charges (Supporting Information). Nonetheless, the minor contribution from the T_1 excited state cannot be completely excluded. The comparison of the QM/MM and isolated-molecule calculation results with experiments shown in Table 2 indicates that the Rh···Rh distance should decrease

Table 2. Comparison of Rh···Rh Distances in the Ground (S_0) and Excited (S_1 and T_1) States[a]

	Rh···Rh distance, $d_{Rh\cdots Rh}$ (Å)		
electronic state	experimental	QM/MM	isolated dimer
S_0	3.379(4)	3.486	3.495
S_1	3.19(1)	3.205	2.971
T_1	–	3.195	2.816

[a]Theoretical geometries of DFT(CAM-B3LYP) with 6-31G** (C, H, O, N, Br)/LANL2DZ (Rh); crystal environment modeled with the Universal Force Field approximation in QM/MM.

upon excitation of excited singlet state S_1 and even more for a potential triplet state T_1. In the case of the optimized isolated dimer, its components are slightly farther apart in the ground state, while upon excitation to S_1 or T_1, the Rh···Rh distance shortens significantly more compared to the solid-state results, by ∼0.4 Å for S_1 and >0.55 Å for T_1. It should also be noted that although the QM/MM-optimized structure for the ground state does not fully match the experimental value, the chosen level of theory yields a sensible excited-state geometry (Supporting Information). Indeed, the experimental and predicted Rh···Rh distances in the S_1 state are statistically consistent. The investigations show that reliable experimental results are extremely important in the case of modeling of excited-state species (Supporting Information).

Overall, the experimental results indicate the formation of an excimer upon near-ultraviolet light irradiation of the **Rh-4-Br** crystal. To date, only one other excimer was detected using the (monochromatic) TR diffraction technique.[70] However, in that case, the bonding situation is far more complex due to the presence of infinite molecular stacks in the crystal structure; thus, the nature of the laser-generated species remains unclear. The excited-state population of **Rh-4-Br** was estimated to be ∼1%, while its lifetime was estimated to be 2 ns at 100 K (no TADF signal was detected). Hence, this is the shortest-living species caught in a time-resolved X-ray Laue experiment so far.[21−25,27,28,31−33,71] This was further evidenced during the pump−probe Laue experiment by the lack of a detectable differential signal 1 ns after laser excitation. Theoretical computations indicated the presence of mixed MLCT and $\pi \rightarrow \pi^*$ transitions and some metal-to-metal bond CT contribution. Nevertheless, as opposed to other works on the Rh···Rh distance contractions,[24−26] on the basis of the spectroscopic features, short TR Laue signal, and theoretical predictions, the refined excited-state model of **Rh-4-Br** can most likely be attributed to the lowest-lying S_1 singlet state. In the previously reported cases of Rh···Rh shortening, often the information about the systems was not fully consistent (e.g., the ES lifetime was determined at a temperature different from that of the TR Laue experiment), and the S_1 excited state was not taken into consideration, even though the 100 ps time delay with the 100 ps-long probe was applied. In this work, excited states S_1 and T_1 were modeled and analyzed, and the increase in the temperature of the sample upon excitation was estimated. The study shows that using the TR Laue method and newly developed processing schemes, it is possible to detect and refine very short-lived excited-state species with close-to-residual populations. We believe that with the ongoing emergence of XFELs, our efforts will contribute to the development of the methods and the design of approximately femtosecond pump−probe experiments in the future.

■ ASSOCIATED CONTENT

Supporting Information

The Supporting Information is available free of charge at https://pubs.acs.org/doi/10.1021/acs.jpclett.4c02476.

Structural, photocrystallographic, spectroscopic, and computational details and relevant figures (PDF)

Crystallographic information (CIF)

■ AUTHOR INFORMATION

Corresponding Authors

Alice Brink − *Department of Chemistry, University of the Free State, Bloemfontein 9301, South Africa*; Email: brinka@ufs.ac.za

Katarzyna N. Jarzembska − *Department of Chemistry, University of Warsaw, 02-089 Warsaw, Poland*; orcid.org/0000-0003-4026-1849; Email: katarzyna.jarzembska@uw.edu.pl

Authors

Piotr Łaski − *Department of Chemistry, University of Warsaw, 02-089 Warsaw, Poland*

Lerato Bosman − *Department of Chemistry, University of the Free State, Bloemfontein 9301, South Africa*

Jakub Drapała − *Department of Chemistry, University of Warsaw, 02-089 Warsaw, Poland; Faculty of Chemistry, Warsaw University of Technology, 00-664 Warsaw, Poland*; orcid.org/0000-0002-5885-6958

https://doi.org/10.1021/acs.jpclett.4c02476
J. Phys. Chem. Lett. 2024, 15, 10301−10306

Radosław Kamiński – *Department of Chemistry, University of Warsaw, 02-089 Warsaw, Poland;* orcid.org/0000-0002-8450-0955

Dariusz Szarejko – *Department of Chemistry, University of Warsaw, 02-089 Warsaw, Poland*

Patryk Borowski – *Department of Chemistry, University of Warsaw, 02-089 Warsaw, Poland;* orcid.org/0000-0003-3848-3506

Andreas Roodt – *Department of Chemistry, University of the Free State, Bloemfontein 9301, South Africa;* orcid.org/0000-0002-7349-6436

Robert Henning – *Center for Advanced Radiation Sources, University of Chicago, Chicago, Illinois 60637, United States*

Complete contact information is available at: https://pubs.acs.org/10.1021/acs.jpclett.4c02476

Notes

The authors declare no competing financial interest.

■ ACKNOWLEDGMENTS

The SONATA BIS grant (2020/38/E/ST4/00400) from the National Science Centre (Poland), the University of the Free State, the National Research Foundation (South Africa; SA NRF) (107802), the Competitive Program for Rated Researchers of SA NRF (111698 and 137759), and the Swiss National Science Foundation (IZLSZ2_149029/1) are acknowledged for financial support. WCSS (Grant No. 285) is thanked for providing computational facilities. The research used resources of APS, a U.S. Department of Energy (DOE) Office of Science User Facility operated for the DOE Office of Science by Argonne National Laboratory (DE-AC02-06CH11357). BioCARS is supported by the National Institute of General Medical Sciences of the National Institutes of Health (NIH) (R24GM111072). The TR setup at Sector 14 was funded in part through collaboration with P. Anfinrud (NIH, National Institute of Diabetes and Digestive and Kidney Diseases).

■ ABBREVIATIONS

XFEL, X-ray free-electron laser; HOMO, highest occupied molecular orbital; LUMO, lowest unoccupied molecular orbital; CT, charge transfer; APS, Advanced Photon Source; GPU, graphical processing unit; QM/MM, quantum mechanics/molecular mechanics

■ REFERENCES

(1) Yam, V. W.-W.; Au, V. K.-M.; Leung, S. Y.-L. Light-Emitting Self-Assembled Materials Based on d^8 and d^{10} Transition Metal Complexes. *Chem. Rev.* **2015**, *115* (15), 7589–7728.

(2) Grätzel, M. Recent advances in sensitized mesoscopic solar cells. *Acc. Chem. Res.* **2009**, *42* (11), 1788–1798.

(3) Coggins, M. K.; Meyer, T. J. Dye Sensitized Photoelectrosynthesis Cells for Making Solar Fuels: From Basic Science to Prototype Devices. In *Photoelectrochemical Solar Fuel Production*; Giménez, S., Bisquert, J., Eds.; Springer: Cham, Switzerland, 2016; pp 513–548.

(4) Mustroph, H.; Stollenwerk, M.; Bressau, V. Current developments in optical data storage with organic dyes. *Angew. Chem., Int. Ed.* **2006**, *45* (13), 2016–2035.

(5) Kamtekar, K. T.; Monkman, A. P.; Bryce, M. R. Recent advances in white organic light-emitting materials and devices (WOLEDs). *Adv. Mater.* **2010**, *22* (5), 572–582.

(6) Pandey, S.; Poudyal, I.; Malla, T. N. Pump-probe time-resolved serial femtosecond crystallography at X-ray free electron lasers. *Crystals* **2020**, *10* (7), 628.

(7) Tenboer, J.; Basu, S.; Zatsepin, N.; Pande, K.; Milathianaki, D.; Frank, M.; Hunter, M.; Boutet, S.; Williams, G.; Koglin, J.; Oberthuer, D.; Heymann, M.; Kupitz, C.; Conrad, C.; Coe, J.; RoyChowdhury, S.; Weierstall, U.; James, D.; Wang, D.; Schmidt, M.; et al. Time-Resolved Serial Crystallography Captures High Resolution Intermediates of Photoactive Yellow Protein. *Science* **2014**, *346* (6214), 1242–1246.

(8) Chen, L. X.; Shelby, M. L.; Lestrange, P. J.; Jackson, N. E.; Haldrup, K.; Mara, M. W.; Stickrath, A. B.; Zhu, D.; Lemke, H.; Chollet, M.; Hoffman, B. M.; Li, X. Imaging ultrafast excited state pathways in transition metal complexes by X-ray transient absorption and scattering using X-ray free electron laser source. *Farad. Discuss.* **2016**, *194* (0), 639–658.

(9) Jarzembska, K. N.; Kamiński, R. Time resolved structural studies in molecular materials. In *Comprehensive Inorganic Chemistry III*, 3rd ed.; Reedijk, J., Poeppelmeier, K. R., Eds.; Elsevier: Oxford, U.K., 2023; pp 273–310.

(10) Deresz, K. A.; Łaski, P.; Kamiński, R.; Jarzembska, K. N. Advances in diffraction studies of light-induced transient species in molecular crystals and selected complementary techniques. *Crystals* **2021**, *11* (11), 1345.

(11) Coppens, P. Molecular excited-state structure by time-resolved pump-probe X-ray diffraction. What is new and what are the prospects for further progress? *J. Phys. Chem. Lett.* **2011**, *2* (2), 616–621.

(12) Coppens, P.; Benedict, J. B.; Messerschmidt, M.; Novozhilova, I.; Graber, T.; Chen, Y.-S.; Vorontsov, I.; Scheins, S.; Zheng, S.-L. Time-resolved synchrotron diffraction and theoretical studies of very short-lived photo-induced molecular species. *Acta Crystallogr., Sect. A* **2010**, *66* (2), 179–188.

(13) Ren, Z.; Bourgeois, D.; Helliwell, J. R.; Moffat, K.; Šrajer, V.; Stoddard, B. L. Laue crystallography: coming of age. *J. Synchrotron Rad.* **1999**, *6*, 891–917.

(14) Hajdu, J.; Johnson, L. N. Progress with Laue diffraction studies on protein and virus crystals. *Biochemistry* **1990**, *29* (7), 1669–1678.

(15) Ihee, H.; Rajagopal, S.; Šrajer, V.; Pahl, R.; Anderson, S.; Schmidt, M.; Schotte, F.; Anfinrud, P. A.; Wulff, M.; Moffat, K. Visualizing reaction pathways in photoactive yellow protein from nanoseconds to seconds. *Proc. Natl. Acad. Sci. U.S.A.* **2005**, *102* (20), 7145–7150.

(16) Moreno-Chicano, T.; Carey, L. M.; Axford, D.; Beale, J. H.; Doak, R. B.; Duyvesteyn, H. M. E.; Ebrahim, A.; Henning, R. W.; Monteiro, D. C. F.; Myles, D. A.; Owada, S.; Sherrell, D. A.; Straw, M. L.; Srajer, V.; Sugimoto, H.; Tono, K.; Tosha, T.; Tews, I.; Trebbin, M.; Strange, R. W.; Weiss, K. L.; Worrall, J. A. R.; Meilleur, F.; Owen, R. L.; Ghiladi, R. A.; Hough, M. A. Complementarity of neutron, XFEL and synchrotron crystallography for defining the structures of metalloenzymes at room temperature. *IUCrJ.* **2022**, *9* (5), 610–624.

(17) Schmidt, M. Biological function investigated by time-resolved structure determination. *Struct. Dyn.* **2023**, *10* (1), 010901.

(18) Schulz, E. C.; Yorke, B. A.; Pearson, A. R.; Mehrabi, P. Best practices for time-resolved serial synchrotron crystallography. *Acta Cryst. Sect. D* **2022**, *78* (1), 14–29.

(19) Schmidt, M. Macromolecular movies, storybooks written by nature. *Biophys. Rev.* **2021**, *13* (6), 1191–1197.

(20) Henning, R. W.; Kosheleva, I.; Šrajer, V.; Kim, I.-S.; Zoellner, E.; Ranganathan, R. BioCARS: Synchrotron facility for probing structural dynamics of biological macromolecules. *Struct. Dyn.* **2024**, *11* (1), 014301.

(21) Jarzembska, K. N.; Hapka, M.; Kamiński, R.; Bury, W.; Kutniewska, S. E.; Szarejko, D.; Szczęśniak, M. M. On the nature of luminescence thermochromism of multinuclear copper(I) benzoate complexes in the crystalline state. *Crystals* **2019**, *9* (1), 36.

(22) Jarzembska, K. N.; Kamiński, R.; Fournier, B.; Trzop, E.; Sokolow, J. D.; Henning, R.; Chen, Y.; Coppens, P. Shedding light on the photochemistry of coinage-metal phosphorescent materials: a time-resolved Laue diffraction study of an Ag^I-Cu^I tetranuclear complex. *Inorg. Chem.* **2014**, *53* (19), 10594–10601.

(23) Makal, A.; Benedict, J.; Trzop, E.; Sokolow, J.; Fournier, B.; Chen, Y.; Kalinowski, J. A.; Graber, T.; Henning, R.; Coppens, P.

Restricted photochemistry in the molecular solid state: structural changes on photoexcitation of Cu(I) phenanthroline metal-to-ligand charge transfer (MLCT) complexes by time-resolved diffraction. *J. Phys. Chem. A* **2012**, *116* (13), 3359−3365.

(24) Makal, A.; Trzop, E.; Sokolow, J.; Kalinowski, J.; Benedict, J.; Coppens, P. The development of Laue techniques for single-pulse diffraction of chemical complexes: time-resolved Laue diffraction on a binuclear rhodium metal-organic complex. *Acta Crystallogr., Sect. A* **2011**, *67* (4), 319−326.

(25) Benedict, J. B.; Makal, A.; Sokolow, J. D.; Trzop, E.; Scheins, S.; Henning, R.; Graber, T.; Coppens, P. Time-resolved Laue diffraction of excited species at atomic resolution: 100 ps single-pulse diffraction of the excited state of the organometallic complex $Rh_2(\mu$-$PNP)_2(PNP)_2$•BPh_4. *Chem. Commun.* **2011**, *47* (6), 1704−1706.

(26) Coppens, P.; Gerlits, O.; Vorontsov, I. I.; Kovalevsky, A. Y.; Chen, Y.-S.; Graber, T.; Gembicky, M.; Novozhilova, I. V. A very large Rh-Rh bond shortening on excitation of the $[Rh_2$(1,8-diisocyano-p-menthane)$4]^{2+}$ ion by time-resolved synchrotron X-ray diffraction. *Chem. Commun.* **2004**, *19* (19), 2144−2145.

(27) Trzop, E.; Fournier, B.; Jarzembska, K.; Sokolow, J.; Kaminski, R.; Benedict, J.; Chen, Y.; Henning, R.; Coppens, P. Selective time-dependent changes of Cu(DPPE)(DMP)·PF_6 on photoexcitation. *Acta Crystallogr., Sect. A* **2014**, *70*, C776.

(28) Coppens, P.; Sokolow, J.; Trzop, E.; Makal, A.; Chen, Y. On the biexponential decay of the photoluminescence of the two crystallographically-independent molecules in crystals of $[Cu(I)(phen)(PPh_3)_2][BF_4]$. *J. Phys. Chem. Lett.* **2013**, *4* (4), 579−582.

(29) Hallmann, J.; Morgenroth, W.; Paulmann, C.; Davaasambuu, J.; Kong, Q.; Wulff, M.; Techert, S. Time-resolved X-ray diffraction of the photochromic α-styrylpyrylium trifluoromethanesulfonate crystal films reveals ultrafast structural switching. *J. Am. Chem. Soc.* **2009**, *131* (41), 15018−15025.

(30) Kang, J.; Lee, Y.; Lee, S.; Ki, H.; Kim, J.; Gu, J.; Cha, Y.; Heo, J.; Lee, K. W.; Kim, S. O.; Park, J.; Park, S.-Y.; Kim, S.; Ma, R.; Eom, I.; Kim, M.; Kim, J.; Lee, J. H.; Ihee, H. Dynamic three-dimensional structures of a metal-organic framework captured with femtosecond serial crystallography. *Nat. Chem.* **2024**, *16* (5), 693−699.

(31) Velazquez-Garcia, J. d. J.; Basuroy, K.; Storozhuk, D.; Wong, J.; Demeshko, S.; Meyer, F.; Henning, R.; Techert, S. Structural dynamics of a thermally silent triiron(ii) spin crossover defect grid complex. *Dalton Trans.* **2023**, *52* (35), 12224−12234.

(32) Velazquez-Garcia, J. d. J.; Basuroy, K.; Storozhuk, D.; Wong, J.; Demeshko, S.; Meyer, F.; Henning, R.; Techert, S. Short- vs. long-range elastic distortion: structural dynamics of a $[2 \times 2]$ tetrairon(II) spin crossover grid complex observed by time-resolved X-Ray crystallography. *Dalton Trans.* **2022**, *51* (46), 17558−17566.

(33) Velazquez-Garcia, J. d. J.; Basuroy, K.; Storozhuk, D.; Wong, J.; Demeshko, S.; Meyer, F.; Henning, R.; Techert, S. Metal-to-metal communication during the spin state transition of a $[2 \times 2]$ Fe(II) metallogrid at equilibrium and out-of-equilibrium conditions. *Dalton Trans.* **2022**, *51* (15), 6036−6045.

(34) Hoshino, M.; Nozawa, S.; Sato, T.; Tomita, A.; Adachi, S.-i.; Koshihara, S.-y. Time-resolved X-ray crystal structure analysis for elucidating the hidden 'over-neutralized' phase of TTF-CA. *RSC Adv.* **2013**, *3* (37), 16313−16317.

(35) Haynes, A. Chapter 1 - Catalytic Methanol Carbonylation. *Adv. Catal.* **2010**, *53*, 1−45.

(36) Hong, J.-H. Two Carbonylations of Methyl Iodide and Trimethylamine to Acetic acid and *N, N*-Dimethylacetamide by Rhodium(I) Complex: Stability of Rhodium(I) Complex under Anhydrous Condition. *Catalysts* **2015**, *5* (4), 1969−1982.

(37) Thomas, C. M.; Süss-Fink, G. Ligand effects in the rhodium-catalyzed carbonylation of methanol. *Coord. Chem. Rev.* **2003**, *243* (1), 125−142.

(38) Maitlis, P. M.; Haynes, A.; Sunley, G. J.; Howard, M. J. Methanol carbonylation revisited: thirty years on. *J. Chem. Soc., Dalton Trans.* **1996**, No. 11, 2187−2196.

(39) Mokolokolo, P. P.; Brink, A.; Roodt, A.; Schutte-Smith, M. Subtle variation of stereo-electronic effects in rhodium(I) carbonyl Schiff base complexes and their iodomethane oxidative addition kinetics. *J. Coord. Chem.* **2020**, *73* (17−19), 2740−2762.

(40) Roodt, A.; Visser, H. G.; Brink, A. Structure/reactivity relationships and mechanism from X-ray data and spectroscopic kinetic analysis. *Crystallogr. Rev.* **2011**, *17* (4), 241−280.

(41) Brink, A.; Roodt, A.; Steyl, G.; Visser, H. G. Steric vs. electronic anomaly observed from iodomethane oxidative addition to tertiary phosphine modified rhodium(I) acetylacetonato complexes following progressive phenyl replacement by cyclohexyl $[PR_3 = PPh_3, PPh_2Cy, PPhCy_2$ and $PCy_3]$. *Dalton Trans.* **2010**, *39* (23), 5572−5578.

(42) Conradie, M. M.; van Rooyen, P. H.; Pretorius, C.; Roodt, A.; Conradie, J. Rhodium-rhodium interactions in [Rh(β-diketonato)-$(CO)_2$] complexes. *J. Mol. Struct.* **2017**, *1144*, 280−289.

(43) Pretorius, C.; Brink, A.; Roodt, A. Crystal structure of acetopyruvato-κ^2*O, O'*-dicarbonylrhodium(I), $C_8H_7O_6Rh$. *Z. Kristallogr. NCS* **2014**, *229* (4), 371−372.

(44) Laurila, E.; Tatikonda, R.; Oresmaa, L.; Hirva, P.; Haukka, M. Metallophilic interactions in stacked dinuclear rhodium 2,2′-biimidazole carbonyl complexes. *CrystEngComm* **2012**, *14* (24), 8401−8408.

(45) Laurila, E.; Oresmaa, L.; Hassinen, J.; Hirva, P.; Haukka, M. Neutral one-dimensional metal chains consisting of alternating anionic and cationic rhodium complexes. *Dalton Trans.* **2013**, *42* (2), 395−398.

(46) Pinter, P.; Soellner, J.; Strassner, T. Metallophilic Interactions in Bimetallic Cyclometalated Platinum(II) N-Heterocyclic Carbene Complexes. *Eur. J. Inorg. Chem.* **2021**, *2021* (30), 3104−3107.

(47) Cechin, C. N.; Paz, A. V.; Piquini, P. C.; Bevilacqua, A. C.; Pineda, N. R.; Fagundes, N. V.; Abram, U.; Lang, E. S.; Tirloni, B. Intermolecular metallophilic interactions in palladium(II) chalcogenolate compounds - An experimental and theoretical study. *Polyhedron* **2020**, *177*, 114315.

(48) Raju, S.; Singh, H. B.; Butcher, R. J. Metallophilic interactions: observations of the shortest metallophilicinteractions between closed shell ($d^{10}\cdots d^{10}$, $d^{10}\cdots d^8$, $d^8\cdots d^8$) metal ions [M···M′ M = Hg(II) and Pd(II) and M′ = Cu(I), Ag(I), Au(I), and Pd(II)]. *Dalton Trans.* **2020**, *49* (26), 9099−9117.

(49) Bergmann, L.; Hedley, G. J.; Baumann, T.; Bräse, S.; Samuel, I. D. W. Direct observation of intersystem crossing in a thermally activated delayed fluorescence copper complex in the solid state. *Sci. Adv.* **2016**, *2* (1), No. e1500889.

(50) Yanai, T.; Tew, D.; Handy, N. A new hybrid exchange-correlation functional using the Coulomb-attenuating method (CAM-B3LYP). *Chem. Phys. Lett.* **2004**, *393* (1−3), 51−57.

(51) Graber, T.; Anderson, S.; Brewer, H.; Chen, Y.-S.; Cho, H.; Dashdorj, N.; Henning, R. W.; Kosheleva, I.; Macha, G.; Meron, M.; Pahl, R.; Ren, Z.; Ruan, S.; Schotte, F.; Šrajer, V.; Viccaro, P. J.; Westferro, F.; Anfinrud, P.; Moffat, K. BioCARS: a synchrotron resource for time-resolved X-ray science. *J. Synchrotron Rad.* **2011**, *18* (4), 658−670.

(52) Coppens, P.; Pitak, M.; Gembicky, M.; Messerschmidt, M.; Scheins, S.; Benedict, J. B.; Adachi, S.-I.; Sato, T.; Nozawa, S.; Ichiyanagi, K.; Chollet, M.; Koshihara, S.-Y. The RATIO method for time-resolved Laue crystallography. *J. Synchrotron Rad.* **2009**, *16* (2), 226−230.

(53) Szarejko, D.; Kamiński, R.; Łaski, P.; Jarzembska, K. N. Seed-skewness algorithm for X-ray diffraction signal detection in the time-resolved synchrotron Laue photocrystallography. *J. Synchrotron Rad.* **2020**, *27* (2), 405−413.

(54) Coppens, P.; Makal, A.; Fournier, B.; Jarzembska, K. N.; Kamiński, R.; Basuroy, K.; Trzop, E. A priori checking of the light-response and data quality before extended data collection in pump-probe photocrystallography experiments. *Acta Cryst. Sect. B* **2017**, *73* (1), 23−26.

(55) Kalinowski, J. A.; Fournier, B.; Makal, A.; Coppens, P. The LaueUtil toolkit for Laue photocrystallography. II. Spot finding and integration. *J. Synchrotron Rad.* **2012**, *19* (4), 637−646.

(56) Kalinowski, J. A.; Makal, A.; Coppens, P. The LaueUtil toolkit for Laue photocrystallography: I. Rapid orientation matrix determi-

nation for intermediate size unit-cell Laue data. *J. Appl. Crystallogr.* **2011**, *44* (6), 1182−1189.
(57) Fournier, B.; Sokolow, J.; Coppens, P. Analysis of multicrystal pump-probe data sets. II. Scaling of ratio data sets. *Acta Crystallogr., Sect. A* **2016**, *72* (2), 250−260.
(58) Coppens, P.; Fournier, B. On the scaling of multicrystal data sets collected at high-intensity X-ray and electron sources. *Struct. Dyn.* **2015**, *2* (6), 064101.
(59) Fournier, B.; Coppens, P. Analysis of multicrystal pump-probe data sets. I. Expressions for the RATIO model. *Acta Crystallogr., Sect. A* **2014**, *70* (5), 514−517.
(60) Coppens, P.; Fournier, B. New methods in time-resolved Laue pump-probe crystallography at synchrotron sources. *J. Synchrotron Rad.* **2015**, *22* (2), 280−287.
(61) Fournier, B.; Coppens, P. On the assessment of time-resolved diffraction results. *Acta Crystallogr., Sect. A* **2014**, *70* (3), 291−299.
(62) Schmøkel, M. S.; Kamiński, R.; Benedict, J. B.; Coppens, P. Data scaling and temperature calibration in time-resolved photo-crystallographic experiments. *Acta Crystallogr., Sect. A* **2010**, *66* (6), 632−636.
(63) Kamiński, R.; Graber, T.; Benedict, J. B.; Henning, R.; Chen, Y.-S.; Scheins, S.; Messerschmidt, M.; Coppens, P. Optimizing the accuracy and precision of the single-pulse Laue technique for synchrotron photo-crystallography. *J. Synchrotron Rad.* **2010**, *17* (4), 479−485.
(64) Cailleau, H.; Lorenc, M.; Guérin, L.; Servol, M.; Collet, E.; Buron-Le Cointe, M. Structural dynamics of photoinduced molecular switching in the solid state. *Acta Crystallogr., Sect. A* **2010**, *66* (2), 189−197.
(65) Vorontsov, I.; Pillet, S.; Kamiński, R.; Schmøkel, M. S.; Coppens, P. *LASER* - a program for response-ratio refinement of time-resolved diffraction data. *J. Appl. Crystallogr.* **2010**, *43* (5), 1129−1130.
(66) Vorontsov, I. I.; Coppens, P. On the refinement of time-resolved diffraction data: comparison of the random-distribution and cluster-formation models and analysis of the light-induced increase in the atomic displacement parameters. *J. Synchrotron Rad.* **2005**, *12* (4), 488−493.
(67) Ozawa, Y.; Pressprich, M. R.; Coppens, P. On the analysis of reversible light-induced changes in molecular crystals. *J. Appl. Crystallogr.* **1998**, *31* (2), 128−135.
(68) Coppens, P.; Kamiński, R.; Schmøkel, M. S. On *R* factors for dynamic structure crystallography. *Acta Crystallogr., Sect. A* **2010**, *66* (5), 626−628.
(69) Rappé, A. K.; Casewit, C. J.; Colwell, K. S.; Goddard, W. A. G., III; Skiff, W. M. UFF, a full periodic-table force-field for molecular mechanics and molecular-dynamics simulations. *J. Am. Chem. Soc.* **1992**, *114* (25), 10024−10035.
(70) Vorontsov, I. I.; Kovalevsky, A. Y.; Chen, Y.-S.; Graber, T.; Gembicky, M.; Novozhilova, I. V.; Omary, M. A.; Coppens, P. Shedding light on the structure of a photoinduced transient excimer by time-resolved diffraction. *Phys. Rev. Lett.* **2005**, *94* (19), 193003.
(71) Basuroy, K.; Velazquez-Garcia, J. d. J.; Storozhuk, D.; Henning, R.; Gosztola, D. J.; Thekku Veedu, S.; Techert, S. Axial vs equatorial: Capturing the intramolecular charge transfer state geometry in conformational polymorphic crystals of a donor-bridge-acceptor dyad in nanosecond-time-scale. *J. Chem. Phys.* **2023**, *158* (5), 054304.

https://doi.org/10.1021/acs.jpclett.4c02476
J. Phys. Chem. Lett. 2024, 15, 10301−10306